CHEMSUKA

CHEMSUKA:
Journal of Chemical Science and Applications

Journal homepage: https://ejournal.uin-suka.ac.id/saintek/chemsuka

Research Article

Synthesis of SnO_2 Nanoparticles by Microwave-Assisted Hydrothermal Method for the Photodegradation of Congo Red Dye

Natasha Shafarossa Marhaendra[1] and Dyah Purwaningsih[1,*]

[1] Department of Chemistry, Universitas Negeri Yogyakarta, Yogyakarta, Indonesia

* Corresponding author: dyah_purwaningsih@uny.ac.id

ABSTRACT

Textile dyes are widely used in manufacturing processes and are often discharged as untreated wastewater, leading to environmental contamination. Congo Red, one of the most common azo dyes found in textile effluents, is highly resistant to conventional treatment methods. Photocatalytic degradation offers an environmentally friendly alternative by utilizing semiconductor-based photocatalysts. In this study, tin oxide (SnO_2) nanoparticles were synthesized via a microwave-assisted hydrothermal method, with the heating duration varied to determine the optimum reaction time. The synthesized nanoparticles were characterized using X-ray diffraction and were applied for the removal of Congo Red through a two steps process: adsorption followed by photocatalytic degradation, with persulfate ions were used as electron scavengers to enhance the degradation efficiency. The results indicate that the microwave-assisted method successfully produced SnO_2 nanoparticles, with the samples synthesized over four hours exhibiting optimal performance. This material exhibited a tetragonal crystal structure with a crystallite size of 8.1 nm and an optical band gap of 3.04 eV. The removal of congo Red via adsorption reached 11.11%. Photocatalytic treatment alone achieved 74.67% degradation, which increased significantly to 98.64% with the addition of persulfate. These findings demonstrate the potential of SnO_2 nanoparticles derived from the microwave-assisted hydrothermal method for efficient dye removal in wastewater treatment.

Keywords: SnO_2 Nanoparticles, Photodegradation, Microwave-Assisted Hydrothermal, Congo Red

1. INTRODUCTION

Textile industry generates large volumes of wastewater containing persistent synthetic dyes [1]. Dyeing and finishing processes contribute 17–20% of industrial wastewater, with an estimated 300,000 tons of synthetic dyes entering aquatic systems annually [2,3]. These pollutants reduce water quality, inhibit photosynthesis, and pose toxicological risks to

organisms. Congo Red, a persistent synthetic dye commonly found in textile effluents, shows low degradability under conventional treatment processes [4].

Semiconductor-based photocatalysis is considered a promising green approach as it can mineralize organic pollutants under UV irradiation without generating secondary waste [5]. Among semiconductor-based photocatalysts, Tin(IV) oxide (SnO_2) has been widely investigated for wastewater dye degradation, but its photocatalytic activity remains limited due to rapid charge recombination under UV irradiation [6].

Conventional hydrothermal synthesis has been widely used to prepare SnO_2-based photocatalysts, but it generally requires long reaction times and provides limited control over morphology. Microwave-assisted hydrothermal synthesis offers advantages such as rapid and uniform heating, shorter reaction times, and improved control over particle morphology [7,8].

Ultrasonication is commonly employed in conventional synthesis routes to enhance nucleation and crystal growth, yet its integration with microwave-assisted hydrothermal synthesis for SnO_2 nanoparticle production remains rarely explored. Although pure SnO_2 nanoparticles have been widely employed for photocatalytic dye degradation, performance improvements are primarily achieved through doping or composite formation rather than using external oxidizing agents. Photocatalytic efficiency can be further increased by using persulfate ions ($S_2O_8^{2-}$), which act as electron scavengers [9]. However, systematic investigations combining microwave-assisted hydrothermal synthesis, ultrasonication, and persulfate activation for optimizing SnO_2 nanoparticle properties and photocatalytic performance remain limited.

Based on this background, this work synthesizes SnO_2 nanoparticles using a microwave-assisted hydrothermal method with varying synthesis durations to evaluate their structural and morphological characteristics and photocatalytic performance for Congo Red degradation with and without persulfate activation.

2. EXPERIMENTAL SECTION

2.1 Materials

Tin(II) chloride dihydrate ($SnCl_2 \cdot 2H_2O$, Merck, analytical grade), sodium hydroxide (NaOH, Merck), absolute ethanol, silver nitrate ($AgNO_3$), Congo Red dye, persulfate solution ($S_2O_8^{2-}$), and deionized water were used as received without further purification.

2.2 Instrumentation

The hidrothermal synthesis was carried out using a household microwave oven (Sharp AQUA-S1112S) operating at 400 W. The reaction was performed under the medium power mode, as the internal temperature of the unit was not directly controllable. The crystal structure of the synthesized SnO_2 nanoparticles was characterized by X-ray diffraction (XRD). Morphology and elemental composition were analyzed using scanning electron microscopy coupled with energy-dispersive X-ray spectroscopy (SEM–EDX). A Shimadzu UV-2450 spectrophotometer was used to measure dye concentration, while a Shimadzu UV–Vis–NIR UV-3600 Plus was employed to record optical absorption spectra for band gap estimation. UV irradiation during photodegradation experiments was provided by a Philips Actinic BL lamp (18 W) 365 nm, positioned 30 cm above the sample.

2.3 Procedure

2.3.1 Synthesis of SnO_2 Nanoparticles

$SnCl_2{\cdot}2H_2O$ (6 mmol; 1.354 g) was dissolved in a mixture of 5 mL absolute ethanol and 15 mL deionized water. The pH of the resulting suspension was adjusted to 13 using a 0.1 M NaOH solution and homogenized via ultrasonication for 30 minutes. The mixture was transferred into a Teflon-lined autoclave and heated using microwave-assisted hydrothermal processing at a medium power setting for 4, 6, or 8 hours. The resulting precipitate was collected, washed, dried in a vacuum oven at 80 °C for 1 hour, and calcined at 500 °C for 4 hours followed by 700 °C for 2 hours. The precipitate washing process was carried out using absolute ethanol and deionized water to ensure the absence of residual chloride ions. The filtrate was tested by adding $AgNO_3$ solution, and washing was repeated until no AgCl precipitate was observed.

2.3.2 Determination of Maximum Absorption Wavelength (λ max) of Congo Red

A Congo Red stock solution (100 mg/L) was prepared by dissolving 0.01 g dye in 100 mL deionized water. The stock solution was then diluted to 10 mg/L and scanned using a UV–Vis spectrophotometer to determine the maximum absorption wavelength (λ_{max}), which was used for subsequent concentration measurements.

2.3.3 Preparation of Congo Red Standard Solutions

Standard solutions of 2, 4, 6, 8, and 10 mg/L were prepared by diluting appropriate volumes (2–10 mL) of the stock solution to 100 mL. The absorbance of these standards at the predetermined λ_{max} was measured to generate a calibration curve.

2.3.4 Catalyst Screening (Photodegradation Test)

For photocatalytic screening, 0.050 g of SnO_2 nanoparticles synthesized at 4, 6, or 8 hours was added to 20 mL of 10 mg/L Congo Red. The suspensions were stirred at 150 rpm and irradiated with UV light for 120 minutes. After treatment, the suspensions were centrifuged, and the residual dye concentration was measured by UV–Vis spectrophotometry at λ_{max}. All experiments in this study were performed in triplicate.

2.3.5 Adsorption in Dark Conditions

The best-performing SnO_2 catalyst from the screening test (based on degradation efficiency) was used in adsorption experiments. A total of 0.10 g catalyst was dispersed in 40 mL of 10 mg/L Congo Red and stirred at 150 rpm in the dark to eliminate photogenerated effects. Samples were withdrawn at selected intervals (0, 5, 10, 15, 30, 60, and 120 minutes), centrifuged, and the supernatant was analyzed by UV–Vis spectrophotometry.

2.3.6 Persulfate-Assisted Photodegradation

To evaluate the activation effect of persulfate ions, 0.10 g of SnO_2 was mixed with 40 mL of 10 mg/L Congo Red. Persulfate activator was added by introducing 5 mL of solutions at 3 mg/L and 5 mg/L, respectively. The suspensions were stirred in the dark for 30 minutes to reach adsorption–desorption equilibrium, followed by UV irradiation. Aliquots were collected at predetermined times (0, 5, 10, 15, 30, 60, and 120 minutes), centrifuged, and analyzed to calculate degradation performance.

3. RESULTS AND DISCUSSION

3.1 Synthesis of SnO_2 Nanoparticles

The microwave-assisted hydrothermal (MAH) method was employed to synthesize SnO_2 nanoparticles. Gao et al. [10] demonstrated that the combination of microwave irradiation and hydrothermal conditions can significantly enhance reaction efficiency and promote favorable morphological development compared to conventional hydrothermal synthesis. Unlike external conductive heating, microwave energy is absorbed directly by the reaction medium, enabling uniform volumetric heating, faster nucleation, and a shorter overall reaction time. To validate this advantage in the present system, three different synthesis durations (4, 6, and 8 hours) were applied. The time variation was intended to examine how

far the reaction can be shortened while still achieving complete precursor conversion and to assess the influence of microwave exposure duration on the formation of SnO_2 nanoparticles.

$SnCl_2 \cdot 2H_2O$ (6 mmol) was dissolved in a 1:3 mixture of absolute ethanol and deionized water and stirred until a white colloid formed. The pH was adjusted to 13 using 0.1 M NaOH to ensure complete hydrolysis of the precursor. The solution was sonicated for homogeneous dispersion and then transferred into a sealed Teflon-lined autoclave.

Figure 1. Comparison of SnO_2 powders before furnace heating (left) and after calcination (right).

Following the MAH treatment, solid SnO_2 powders were successfully obtained for all synthesis durations. The material synthesized for 4 hours showed a light grey color, whereas samples prepared for 6 and 8 hours exhibited a pale-yellow appearance. This gradual color transition indicates a more complete thermal conversion of the hydroxide precursor and the progressive removal of residual chloride and surface hydroxyl groups. After drying and calcination, the powders formed fine particulate solids without visible residual precursor or phase separation, suggesting that microwave energy facilitated uniform conversion throughout the reaction volume.

The final calcined samples retained good structural integrity and showed no signs of sintering or melting, indicating that the selected temperature steps were adequate to stabilize the material without damaging its microscale texture. The pale-yellow tone observed after calcination also suggests the presence of oxygen vacancies, which commonly develop during high-temperature processing of SnO_2 and are associated with enhanced surface reactivity. These macroscopic observations confirm that the MAH synthesis combined with controlled post-treatment produced SnO_2 powders suitable for further structural and photocatalytic evaluation.

3.2 XRD Characterization

XRD analysis was employed to determine the crystallite size of the SnO_2 nanoparticles. The diffraction patterns were recorded in the 2θ range of 10°–90°. The obtained diffraction peaks of the synthesized SnO_2 nanoparticles, in terms of their position and intensity, were compared with reference patterns from the International Centre for Diffraction Data (ICDD).

The XRD patterns of the SnO_2 nanoparticles synthesized at different durations confirm the formation of the cassiterite tetragonal phase (ICDD 01-077-0447). All samples show characteristic reflections indexed to the (110), (101), (200), (211), (220), and (310) planes, with the most intense peak at 2θ ≈ 26.6° corresponding to the (110) plane, which is known as the most stable growth orientation for SnO_2 [11]. Small deviations of ±0.1–0.2° relative to the ICDD reference are within normal experimental limits and may originate from lattice strain, crystallite size variations, or residual ionic species such as Cl^- or Na^+ [12].

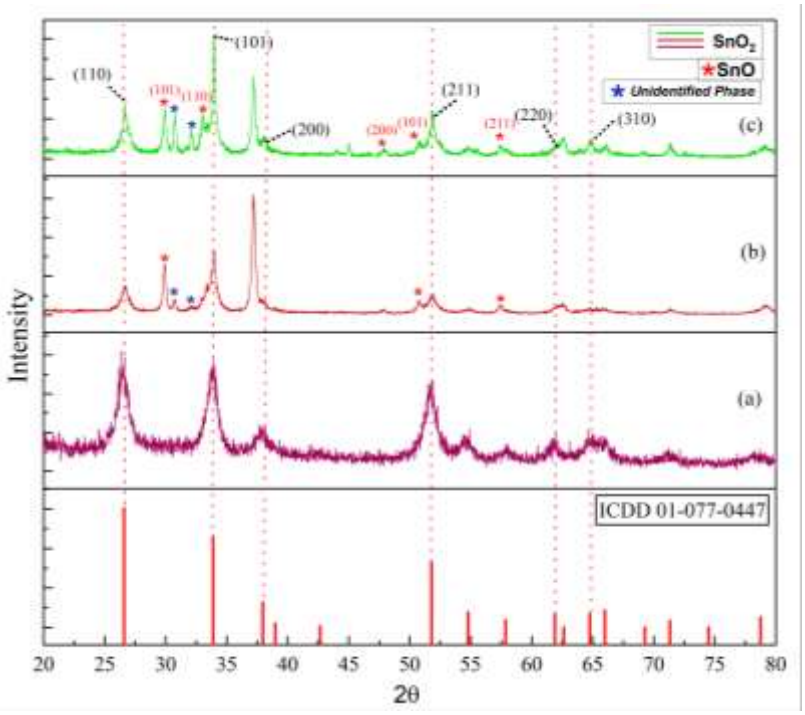

Figure 2. XRD patterns of SnO_2 nanoparticles synthesized for (a) 4, (b) 6, and (c)8 hours

The SnO_2 sample synthesized for 4 hours exhibits broader diffraction peaks, which indicate smaller crystallite size and higher structural disorder. This is consistent with the Scherrer principle, where peak broadening is associated with nanosized domains and lattice imperfections [13]. Smaller crystallites tend to produce stronger quantum size effects, potentially widening the band gap and improving photocatalytic behavior [14]. In contrast, the 6 hours sample shows noticeably sharper and more intense peaks, suggesting higher

crystallinity, lower lattice strain, and more ordered crystal growth. Interestingly, the reflection at the (310) plane is not observable for the 6 hours sample, likely due to preferential orientation or reduced signal intensity for minor planes [15].

The 8 hours sample also displays sharp diffraction peaks, confirming good crystallinity, although prolonged synthesis may promote grain coarsening and particle agglomeration, which can reduce the effective surface area [16]. Additional diffraction peaks were observed in the nanoparticles synthesized for 6 and 8 hours at 2θ values of approximately 29° and 33°, which were attributed to minor SnO phases and unidentified phases based on ICDD references, with intensities significantly lower than that of the dominant SnO_2 phase. The emergence and increasing intensity of these minor phases with prolonged reaction time are associated with oxygen imbalance and lattice defects during synthesis, indicating that a synthesis duration of 4 hours is optimal for obtaining phase-pure SnO_2 nanoparticles.Overall, all samples crystallize in the cassiterite tetragonal structure characterized by a $P4_2/mnm$ space group, where Sn^{4+} ions are octahedrally coordinated by O^{2-}, supporting structural stability and electron transport [17].

The crystallite size can be determined based on the 2θ values and the full width at half maximum (FWHM). The crystallite size was calculated using the Debye–Scherrer equation as follows:

$$D = \frac{K.\lambda}{\beta.cos\theta} \quad (1)$$

where D is the crystallite size, K is the Scherrer constant, λ is the wavelength of the Cu Kα radiation, β is the FWHM of the peak, and θ is the Bragg angle corresponding to the peak position. Based on the calculations using Eq. (1), the crystallite sizes of the SnO_2 nanoparticles synthesized for 4 h, 6 h, and 8 h were 8.1 nm, 14.6 nm, and 22.6 nm, respectively. In relation to the increased synthesis time, the resulting crystallite size also increased, indicating that the crystal growth process proceeded more completely. The thermal energy generated during synthesis allows Sn^{4+} and O^{2-} atoms to arrange into a more stable crystal lattice, resulting in larger crystallite dimensions. These findings indicate that synthesis duration plays a key role in determining crystallite size, defect density, and preferred orientation, ultimately influencing the structural quality and functional performance of SnO_2 nanoparticles.

3.3 SEM-EDX Characterization

SEM analysis of SnO_2 nanoparticles reveals the surface morphology of the samples at different magnifications. SEM images of SnO_2 nanoparticles synthesized for 4 hours show a nanosheet-like morphology across all magnifications. At 1000×, large flat plate structures are visible with small particles attached to their surfaces, indicating secondary aggregation of primary nanoparticles, which is typical of microwave-assisted hydrothermal synthesis [18]. At 3000× and 5000×, the sheets become rougher and covered by fine nodular particles in the sub-micrometer to nanometer range, forming a porous granular layer that increases surface area and provides more active sites for photocatalysis and sensing applications [19,20]. At 10000×, compact nanoparticle clusters with estimated sizes of tens to hundreds of nanometers are observed, suggesting that these primary grains act as building blocks for the nanosheets. Overall, the SEM results confirm the formation of layered SnO_2 nanosheets decorated by nanometric particles, producing a rough surface that may enhance photocatalytic performance through an expanded active surface.

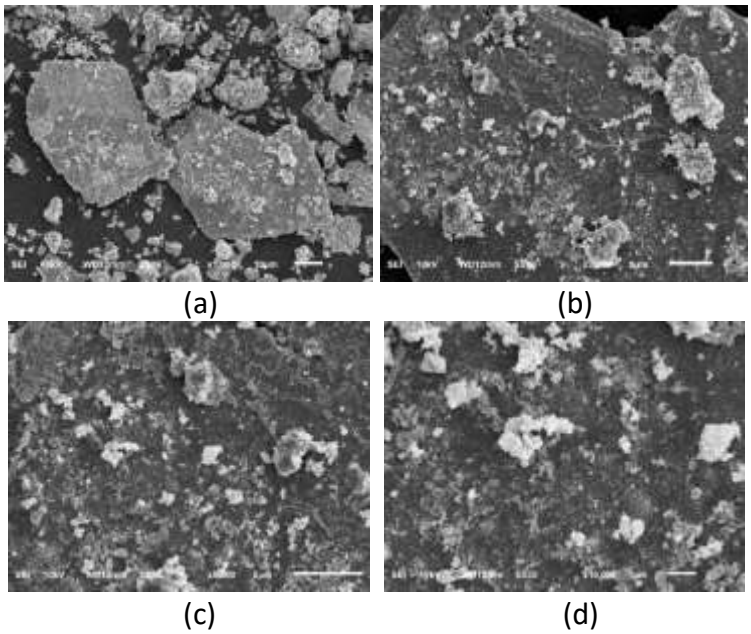

Figure 3. Surface morphology of SnO_2 nanoparticles synthesized for 4 h observed at magnifications of (a) 1000×, (b) 3000×, (c) 5000×, and (d) 10000×.

Meanwhile, EDX provides elemental distribution mapping within the sample [21]. Based on the EDX analysis, two main peaks were observed. The O–Kα peak at 0.525 keV and several characteristic Sn–L peaks starting at 3.442 keV.

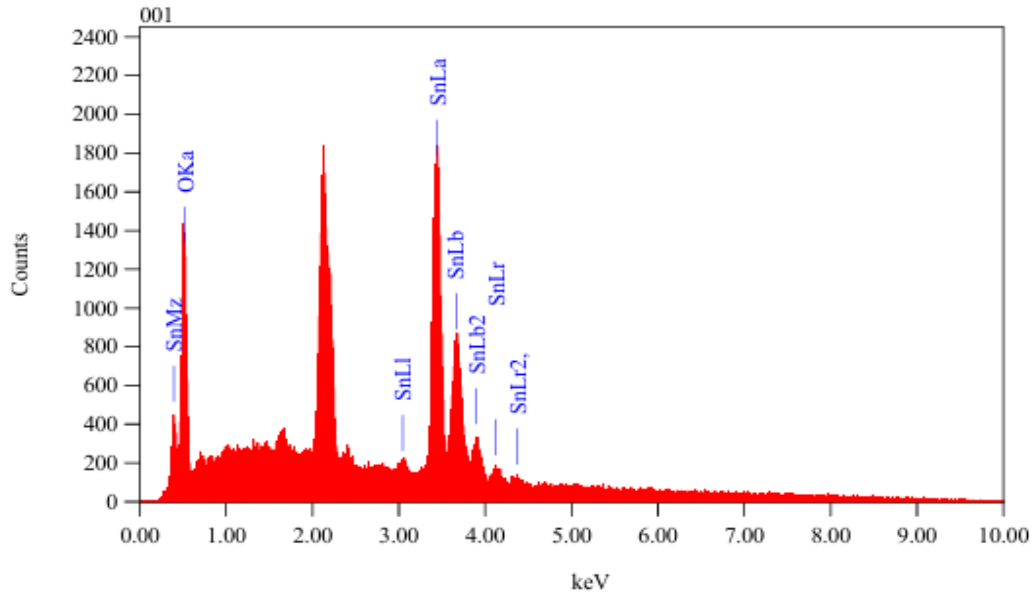

Figure 4. EDX spectrum of the SnO_2 nanoparticles synthesized for 4 hours

Table 1. EDX composition of the SnO_2 nanoparticles synthesized for 4 h

Element	Atomic (%)	Weight (%)
O	66.02%	20.75
Sn	33.98%	79.25

Quantification using the ZAF method shows that the sample consists of 79.25 wt% Sn and 20.75 wt% O. The atomic percentages are 33.98% for Sn and 66.02% for O. The O/Sn ratio is 1.94, which is consistent with the expected stoichiometry of SnO_2 (O:Sn = 2:1). Oxygen atoms are more dominant than tin atoms.

3.4 UV–Vis NIR Spectrophotometric Analysis

Absorbance analysis using a UV–Vis NIR spectrophotometer can be used to determine the bandgap energy of SnO_2 nanoparticles through the measured absorbance. The absorbance spectrum was recorded within the relevant wavelength range, and the bandgap was calculated using the Tauc equation:

$$(\alpha h\nu)^n = A(h\nu - E_g) \quad (2)$$

In this equation, α represents the absorption coefficient, hν is the photon energy (eV), A is the proportionality constant, $E_{(g)}$ is the bandgap energy, and n is set to $\frac{1}{2}$ for SnO_2.

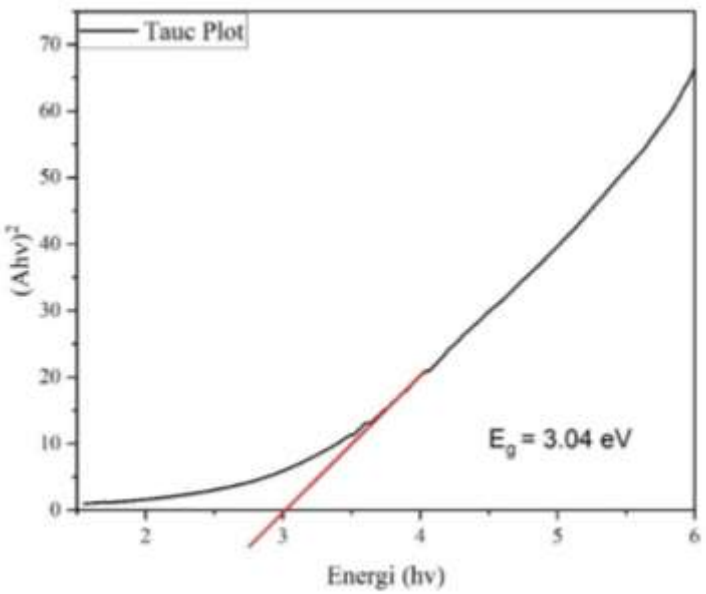

Figure 5. Band Gap Energy Plot of SnO_2 Nanoparticles

The bandgap energy (Eg) was determined using the Tauc plot method. The equation produces a plot of photon energy (hv) versus $(A\ hv)^2$, where the linear region of the curve is extrapolated to the x-axis to obtain the bandgap value. The use of $(A\ hv)^2$ is based on the direct allowed transition characteristic of SnO_2 nanoparticles [22]. The calculated bandgap energy of the synthesized SnO_2 nanoparticles was 3.04 eV, which is lower than that of bulk SnO_2 (3.6–4.0 eV), yet still classified as a wide-bandgap semiconductor. A large Eg value indicates that SnO_2 nanoparticles primarily absorb light in the ultraviolet region, consistent with the optical behavior of metal oxide semiconductors [23].

3.5 Catalyst Screening (Photodegradation Test)

This test was conducted to evaluate the photocatalytic performance of the three SnO_2 nanoparticles synthesized at different synthesis durations. UV irradiation was used in the photodegradation of Congo Red because the photocatalyst employed was pure SnO_2 nanoparticles, which are not sufficiently active under visible light. This is due to the photon energy in the visible spectrum (≈1.6–3.0 eV), which is insufficient to effectively excite electrons from the valence band to the conduction band of SnO_2, thereby limiting the formation of electron–hole pairs required for photodegradation [24].

When the catalyst in the solution is irradiated with UV light of equal or higher energy, electron-hole pairs (e^- and h^+) are generated on the catalyst surface. Electrons (e^-) from the valence band are excited to the conduction band, leaving positive holes (h^+), thereby producing electron–hole pairs. These charge carriers participate in redox reactions that

generate hydroxyl radicals (•OH) and superoxide radicals ($•O_2^-$). Hydroxyl radicals possess strong oxidizing properties and high redox potential, enabling them to oxidize most organic compounds into water, hydroxyl acids, and carbon dioxide [25].

Table 2. Congo Red Measurement Data with SnO_2 Nanoparticles Synthesized for 4 h, 6 h, and 8 h After Irradiation

No	Synthesis Time (h)	Concentration (ppm)	Absorbance
1.	4	2.54	0.16504
2.	6	4.22	0.26878
3.	8	9.85	0.61638

Based on Table 2 were used to calculate the degradation percentage using the following equation:

$$\% D = \frac{C^0 - C}{C^0} \times 100\% \quad (3)$$

In this equation, %D represents the degradation percentage, C_o is the initial concentration of the Congo Red solution, and C is the concentration of the Congo Red solution after irradiation. Based on this Eq. (3), the degradation percentages of the three samples were obtained as follows: 75.10%, 58.64%, 3.52%. The SnO_2 nanoparticles synthesized for 4 hours exhibited the highest degradation percentage of 75.109%, showing a significant difference compared with the samples synthesized for 6 hours and 8 hours. This result is consistent with the XRD characterization, where the 4 hours sample demonstrated smaller crystallite size, better crystallinity, and a larger active surface area, providing more active sites for interaction with Congo Red molecules. Under UV irradiation, SnO_2 generates electrons (e^-) and holes (h^+), which subsequently form reactive radicals such as •OH and $•O_2^-$ that are responsible for breaking the azo bonds in Congo Red, leading to color fading and molecular degradation [26].

3.6 Adsorption in Dark Conditions

Adsorption experiments in the dark were performed to determine the time required to achieve adsorption–desorption equilibrium between the dye and the photocatalyst. This test was also conducted to ensure that photocatalytic degradation did not occur simultaneously with the adsorption process. The dark-condition method was performed by wrapping the Erlenmeyer flask with aluminum foil and stirring the suspension for a predetermined period. The solution was then analyzed for its concentration using a UV–Vis spectrophotometer.

Table 3. Concentration of Congo Red During Dark Adsorption

Time (min)	Concentration (ppm)
0	9.82
5	9.30
10	9.14
15	8.89
30	8.72
60	8.50
120	8.09

The data above show that the concentration of Congo Red decreases with increasing adsorption time. The adsorption kinetics were evaluated using zero-order, first-order, and second-order reaction models:

Zero-order: $C_t = -kt + C_o$ (4)

First-order: $\ln C_t = -kt + \ln C_0$ (5)

Second-order: $^1/_{C_t} = -kt + {}^1/_{C_0}$ (6)

Here, C_t is the Congo Red concentration at time t (ppm), k is the rate constant, t is time (min), and C_o is the initial concentration [27]. The model with the highest R^2 value indicates the reaction order. The determined R^2 values for the zero, first, and second-order models were 0.7767, 0.8029, and 0.8279, respectively. Based on these results, the adsorption process follows a second-order reaction.

The adsorption effectiveness of Congo Red by SnO_2 nanoparticles was calculated using the following equation:

$$\%Effectiveness = \frac{C_0 - C_e}{C_0} \times 100\% \quad (7)$$

where C_o is the initial concentration (ppm) and C_e is the equilibrium concentration [28]. Based on Eq. (7), the adsorption effectiveness of the SnO_2 nanoparticles was 11.11%.

3.7 Persulfate-Assisted Photodegradation

Based on catalyst screening results, an additional strategy is required to enhance the photocatalytic system performance and achieve degradation values above 90%. One widely used approach to support the primary catalyst in photocatalysis is the introduction of an external oxidizing agent, such as persulfate ions, as a co-catalyst [29].

During the UV-assisted dye degradation process, UV light and the SnO_2 nanoparticle photocatalyst activate persulfate ions into sulfate radicals ($SO_4^{\bullet -}$), which possess a high oxidation potential capable of breaking down complex organic compounds [30]. The addition

of persulfate solution is also considered an economical and environmentally friendly method for supporting dye photodegradation, in accordance with green chemistry principles. Persulfate is relatively inexpensive, highly soluble in water, and its reaction by products are environmentally benign [31].

Table 4. Congo Red Concentration (No Persulfate)

Time (min)	Concentration (ppm)
0	8.83
5	8.29
10	7.96
15	7.66
30	7.22
60	5.28
120	2.23

The determined R^2 values for the zero, first, and second-order models were 0.9953, 0.9767, and 0.9194. Based on these results, the adsorption process follows a zero-order reaction. This indicates that the reaction rate does not depend on the dye concentration in solution, but is controlled by light intensity and the number of active sites on the SnO_2 nanoparticle surface. Photodegradation of dyes using SnO_2 photocatalysts generally follows first-order kinetics, as the reaction rate is proportional to the remaining dye concentration during irradiation. This behavior results from the relatively constant amount of oxidative radicals, with the degradation rate being controlled by the substrate concentration [32].

Table 5. Congo Red Concentration (3 mg/L Persulfate)

Time (min)	Concentration (ppm)
0	8.42
5	7.78
10	5.29
15	4.14
30	3.99
60	1.44
120	0.11

The determined R^2 values for the zero, first, and second-order models were 0.7872, 0.9812, and 0.8243. Based on these results, the adsorption process follows a first-order reaction. The addition of persulfate ions ($S_2O_8^{2-}$) changed the reaction order from zero to first order, with an R^2 value of 0.9812. This shift in reaction order indicates that the surface-controlled mechanism is no longer dominant, and the reaction rate becomes dependent on the dye concentration due to the increased formation of oxidative species (•OH and $SO_4•^-$). These radicals accelerate the oxidation process, making the reaction rate proportional to the

remaining dye concentration. Therefore, the addition of persulfate plays a crucial role in enhancing the photocatalytic performance of SnO_2, as reflected in the transition to first-order reaction kinetics.

Table 6. Congo Red Concentration (5 mg/L Persulfate)

Time (min)	Concentration (ppm)
0	8.19
5	7.31
10	5.06
15	4.50
30	3.97
60	3.39
120	2.99

The determined R^2 values for the zero, first, and second-order models were 0.5536, 0.6727, and 0.7917. The reaction order of Congo Red photodegradation with the addition of 5 mg/L persulfate follows second-order kinetics. In this case, the reaction rate is influenced by the concentrations of two reactive species: the dye molecules and the oxidative radicals generated during irradiation. However, the R^2 value is relatively low (<0.8), which is most likely attributed to self-scavenging effects. The sulfate radicals ($SO_4^{\bullet -}$) generated react with each other, resulting in a reduced number of oxidative radicals available to attack the dye molecules.

Based on the linear equations of each curve, the photocatalytic degradation rate without persulfate was calculated using:

$$r = kC^{\mathrm{n}} \quad (8)$$

where r is the reaction rate in ppm/min, C is the concentration in ppm, k is the reaction rate constant, and n is the reaction order [33]. From the regression results, the photocatalytic degradation rate without persulfate was determined to be 0.0536 ppm/min, with 3 mg/L persulfate, the reaction rate increased to 0.2933 ppm/min, while with 5 mg/L persulfate, the reaction rate was 0.1075 ppm/min. In addition, the degradation percentage was calculated using Eq. (3). The degradation percentage without persulfate was 74.67%, with 3 mg/L persulfate it increased to 98.64%, and with 5 mg/L persulfate it decreased to 63.52%.

In previous studies, pure SnO_2 photocatalysts generally showed limited degradation activity under UV irradiation. Paramarta et al. [34] reported that undoped SnO_2 nanoparticles degraded Congo Red only 32.6% after 120 minutes, while Ma et al. [35] achieved 58.8% removal within 45 minutes using precipitation-derived SnO_2. In contrast, the SnO_2

nanoparticles synthesized in this work exhibited 74.67% photodegradation in the absence of persulfate, demonstrating superior activity even without surface modification or composite formation.

When persulfate was introduced into the system, the degradation performance of the catalyst significantly improved. The addition of 3 mg/L $S_2O_8^{2-}$ increased the degradation efficiency from 74.67% to 98.64%, which indicates that persulfate effectively scavenges photogenerated electrons and promotes the formation of $SO_4\bullet^-$ radicals with high oxidation potential. The reaction mechanisms can be described by the following equations:

$$S_2O_8^{2-} + e^- \rightarrow SO_4\bullet^- + SO_4^{2-} \quad (9)$$

A similar trend was reported by Zhang et al. [36] who demonstrated that persulfate activation enhanced dye degradation due to the ability of $SO_4\bullet^-$ to oxidize organic pollutants more efficiently than •OH increasing the removal efficiency of methylene blue from approximately 40% to 95% under UV irradiation.

However, when the persulfate concentration was increased to 5 mg/L, the degradation dropped to 63.52%, which is consistent with the phenomenon of radical self-scavenging commonly observed at excessive oxidant doses, where excess $S_2O_8^{2-}$ consumes active species ($SO_4\bullet^-$/•OH) and competes with dye molecules, thereby suppressing the degradation reaction. The reaction mechanisms can be described by the following equations:

$$SO_4\bullet^- + SO_4\bullet^- \rightarrow S_2O_8^{2-} \quad (10)$$

Wang et al [36] showed that increasing the PDS dosage from 0.5 to 1.0 mmol enhanced phenol degradation from 93% to 98%, whereas a further increase to 1.5–2.0 mmol led to a noticeable decrease in degradation efficiency due to the quenching (self-scavenging) of reactive radicals by excess persulfate.

Based on all the obtained data, the photocatalytic degradation of Congo Red using SnO_2 nanoparticles was most effective with the addition of 3 mg/L persulfate solution. Therefore, the introduction of persulfate can serve as an effective and sustainable supporting strategy for the photodegradation of Congo Red using SnO_2 nanoparticles. In this study, a persulfate concentration of 3 mg/L provided the best performance; however, it should be noted that an optimum persulfate concentration exists in the SnO_2 photocatalytic system, as excessive persulfate addition (5 mg/L) can reduce the degradation efficiency.

4. CONCLUSION

The variation of synthesis time in the microwave-assisted hydrothermal method influenced the characteristics and photocatalytic activity of the resulting SnO_2 nanoparticles. The shorter synthesis duration of 4 hours produced nanoparticles with a more stable structure and demonstrated the highest Congo Red photodegradation performance. The SnO_2 nanoparticles synthesized at the optimum duration (4 hours) exhibited a bandgap energy of 3.04 eV and a crystallite size of 8.1 nm based on XRD calculations. SEM analysis indicated a nanosheet-like morphology with a tetragonal structure, while EDX confirmed the presence of Sn and O elements consistent with the stoichiometry of SnO_2. These physical characteristics verify that the microwave-assisted hydrothermal method successfully produced SnO_2 nanoparticles suitable for photocatalytic applications.

The photodegradation of Congo Red using SnO_2 nanoparticles synthesized at different durations produced the highest degradation percentage of 74.67% for the sample synthesized for 4 hours, following zero-order kinetics. When 3 mg/L persulfate ($S_2O_8^{2-}$) was added, the degradation increased to 98.64% and followed first-order kinetics.

ACKNOWLEDGEMENTS

The authors gratefully acknowledge Universitas Negeri Yogyakarta for providing laboratory facilities and technical support for the completion of this research. The authors also acknowledge Hari Muryanto for language assistance and final draft improvements.

REFERENCES

[1] Bailey, K., Basu, A., & Sharma, S. (2022). The environmental impacts of fast fashion on water quality: A systematic review. *Water*, *14*(7), 1073–1089.

[2] Islam, M. T., Al Mamun, M. A., Halim, A. F. M. F., Peila, R., & Sanchez Ramirez, D. O. (2024). Current trends in textile wastewater treatment—bibliometric review. *Environmental Science and Pollution Research*, *31*(13), 19166–19184.

[3] Phan, K.-H., Le, L.-T., Ninh, T.-T. N., Tran, C.-S., Nguyen, T.-T., Nguyen, D.-T.-D., … Bui, X.-T. (2024). Decolorization and degradation of azo dyes in thermophilic biological wastewater treatment process: A mini-review. *Chemical and Environmental Engineering, 10*, 101018.

[4] Siddiqui, S. I., Allehyani, E. S., Al-Harbi, S. A., Hasan, Z., Abomuti, M. A., Rajor, H. K., & Oh, S. (2023). Investigation of Congo red toxicity towards different living organisms: A review. *Processes, 11*(3), 807.

[5] Ahmed, M. A., & Mohamed, A. A. (2023). Recent progress in semiconductor/graphene photocatalysts: Synthesis, photocatalytic applications, and challenges. *RSC Advances*, *13*(1), 421–439.

[6] Yakout, S. M. (2021). Engineering of visible light photocatalytic activity in SnO2 nanoparticles: Cu2+-integrated Li+, Y3+ or Zr4+ dopants. *Optical Materials, 116*, 111077.

[7] Kumar, A., Kuang, Y., Liang, Z., & Sun, X. (2020). Microwave chemistry, recent advancements, and eco-friendly microwave-assisted synthesis of nanoarchitectures and their applications: A review. *Materials Today Nano*, 11, 100076.

[8] Wu, S., & Dai, W. (2017). Microwave-hydrothermal synthesis of SnO_2-CNTs hybrid nanocomposites with visible light photocatalytic activity. *Nanomaterials, 7*(3), 54.

[9] He, S., Chen, Y., Li, X., Zeng, L., & Zhu, M. (2022). Heterogeneous photocatalytic activation of persulfate for the removal of organic contaminants in water: A critical review. *ACS ES&T Engineering*, *2*(4), 527–546.

[10] Gao, Y., Remón, J., & Matharu, A. S. (2021). Microwave-assisted hydrothermal treatments for biomass valorisation: A critical review. *Green Chemistry*, *23*(10), 3502–3525.

[11] Wu, S., & Dai, W. (2017). Microwave-hydrothermal synthesis of SnO_2-CNTs hybrid nanocomposites with visible light photocatalytic activity. *Nanomaterials, 7*(3), 54.

[12] Sen, S. K., Hossain, M. S., Roy, R., Alam, M. S., Manir, M. S., & Biswas, G. G. (2024). Size–strain distribution analysis from XRD peak profile of (Mg, Fe) co-doped SnO_2 nanoparticles fabricated using chemical co-precipitation route. *Ceramics International, 50*(21C), 44038–44055.

[13] Jannat, M. R., Biswas, B., Rahman, M. L., Ahmed, M. F., Hossain, M. J., Khanam, J., & Sharmin, N. (2025). Validity of crystallite size determination methods based on XRD peak broadening in pure and metal-doped nickel ferrites. *Materials, 28,* 100762.

[14] Mishra, S., Pandey, B. K., Jaiswal, R. L., Gupta, J., & Sachin. (2024). Unified model for the studies of band gap of nanosolids with their varying shape and size. *Chemical Physics Letters, 841*, 141177.

[15] Ali, A., Chiang, Y. W., & Santos, R. M. (2022). X-ray diffraction techniques for mineral characterization: A review for engineers of the fundamentals, applications, and research directions. *Minerals*, *12*(2).

[16] Nurhidayah, E., Yuwono, A. H., Septiningrum, F., Maulana, F. A., Dhaneswara, D., Sofyan, N., Pangesty, A. I., & Noviyanto, A. (2024). *Optimizing the photocatalytic performance of SnO_2 nanoparticles for methylene blue removal with variation in calcination temperatures.* In E3S Web of Conferences, 488, 02016.

[17] Hoang Huy, V. P., Nguyen, T. M. H., & Bark, C. W. (2023). Recent advances of doped SnO_2 as electron transport layer for high-performance perovskite solar cells. *Materials*, *16*(18).

[18] Wang, D., Li, Y., Ding, Y., Jia, X., Zhong, D., Zhang, X., Zhao, J., & Fang, Y. (2023). Facile synthesis of a multifunctional SnO_2 nanoparticles/nanosheets composite for dye-sensitized solar cells. *ACS Omega, 8*(47), 44578–44585.

[19] Araújo, E. S., Pereira, M. F. G., da Silva, G. M. G., Tavares, G. F., Oliveira, C. Y. B., & Faia, P. M. (2023). A review on the use of metal oxide-based nanocomposites for the remediation of organics-contaminated water via photocatalysis: Fundamentals, bibliometric study and recent advances. *Toxics*, *11*(8).

[20] Tasisa, Y. E., Sarma, T. K., Sahu, T. K., & Krishnaraj, R. (2024). Phytosynthesis and characterization of tin-oxide nanoparticles (SnO_2-NPs) from Croton macrostachyus leaf extract and its application under visible light photocatalytic activities. *Scientific Reports, 14*(1), 10780.

[21] Thuan, N. D., Cuong, H. M., Nam, N. H., Lan Huong, N. T., & Hong, H. S. (2024). Morphological analysis of Pd/C nanoparticles using SEM imaging and advanced deep learning. *RSC Advances, 14*(47), 35172–35183.

[22] Gong, J., Wang, X., Fan, X., Dai, R., Wang, Z., Zhang, Z., & Ding, Z. (2019). Temperature dependent optical properties of SnO_2 film studied by ellipsometry. *Optical Materials Express*, *9*(9), 3691–3703.

[23] Bathula, B., Gurugubelli, T. R., Yoo, J., & Yoo, K. (2023). Recent progress in the use of SnO_2 quantum dots: From synthesis to photocatalytic applications. *Catalysts*, 13(4), 765.

[24] Sadik, W., El-Demerdash, A. M., Nashed, A. W., Mostafa, A. A., & Lamie, E. (2024). Synthesis and investigation of optical properties and enhancement photocatalytic activity of TiO_2–SnO_2 semiconductor for degradation of organic compounds. *Scientific Reports, 14*(1), 27846.

[25] Moradi, M., & Saien, J. (2025). Solar activation of persulfate for simultaneous degradation of antibiotic drug and edible dye in a thin-layer flow photo-reactor. *Arabian Journal of Chemistry, 18*, 1–10.

[26] Tan, S. N., Yuen, M. L., & Ramli, R. A. (2025). Photocatalysis of dyes: Operational parameters, mechanisms, and degradation pathway. *Green Analytical Chemistry, 12*, 100230.

[27] Thuan, N. D., Cuong, H. M., Nam, N. H., Lan Huong, N. T., & Hong, H. S. (2024). Morphological analysis of Pd/C nanoparticles using SEM imaging and advanced deep learning. *RSC Advances, 14*(47), 35172–35183.

[28] Kadhium, S. S., AL-Lamei, A. J., & Majed, N. (2021). Removal of E102 dye from aqueous solution by adsorption on the surface of polyaniline walnut husks nanocomposite. *Egyptian Journal of Chemistry*, *64*(9), 4783–4790.

[29] Hasanzadeh, M., Ghaedrahmat, Z., Kayedi, N., Haghighi Fard, N. J., Azari, A., & Afsharizadeh, M. (2023). Persulfate-assisted heterogeneous photocatalytic degradation

of furfural from aqueous solutions using TiO_2–ZnO/biochar composite. *Heliyon*, *9*(11), e21421.

[30] Saien, J., & Jafari, F. (2022). Methods of persulfate activation for the degradation of pollutants: Fundamentals and influencing parameters. *Persulfate-Based Oxidation Processes in Environmental Remediation*, 1–59.

[31] Moradi, M., & Saien, J. (2025). Solar activation of persulfate for simultaneous degradation of antibiotic drug and edible dye in a thin-layer flow photo-reactor. *Arabian Journal of Chemistry, 18*, 1–10.

[32] Shabna, S., Dhas, S. S. J., & Biju, C. S. (2023). Potential progress in SnO_2 nanostructures for enhancing photocatalytic degradation of organic pollutants. *Catalysis Communications, 177*, 106642.

[33] Chiu, Y. H., Chang, T. F. M., Chen, C. Y., Sone, M., & Hsu, Y. J. (2019). Mechanistic insights into photodegradation of organic dyes using heterostructure photocatalysts. *Catalysts*, *9*(5).

[34] Paramarta, V., Taufik, A., Munisa, L., & Saleh, R. (2017). *Sono-and photocatalytic activities of SnO2 nanoparticles for degradation of cationic and anionic dyes.* In AIP Conference Proceedings, 1788, 030125.

[35] Ma, C. M., Hong, G. B., & Lee, S. C. (2020). Facile synthesis of tin dioxide nanoparticles for photocatalytic degradation of Congo red dye in aqueous solution. *Catalysts*, *10*(7), 1–17.

[36] Wang, G., Kou, L., Li, C., Xu, B., & Wu, Y. (2025). Enhanced Degradation of Phenol in Aqueous Solution via Persulfate Activation by Sulfur-Doped Biochar: Insights into Catalytic Mechanisms and Structural Properties. *Nanomaterials, 15*(13), 979.